Nonequilibrium and hysteresis in solids: Disentangling conditioning from nonlinear elasticity

M. Scalerandi,[1] A. S. Gliozzi,[1] C. L. E. Bruno,[2] and P. Antonaci[2]
[1]*Physics Department, Politecnico di Torino, Torino, Italy*
[2]*Structural and Geotechnical Engineering Department, Politecnico di Torino, Torino, Italy*
(Received 25 May 2009; revised manuscript received 2 March 2010; published 29 March 2010)

Elastic hysteresis in solids is a complex matter which may affect a wide range of applications. As observed in rocks, it is the result of the interplay between nonlinear and nonequilibrium phenomena, such as conditioning, relaxation, and memory. Here we will propose a theoretical nondeterministic framework in which nonequilibrium effects are a natural consequence of the model. Experimental results will be shown to demonstrate that the separation of such effects is fundamental to extract truthful information on nonlinearity.

DOI: 10.1103/PhysRevB.81.104114 PACS number(s): 62.20.−x, 43.25.+y, 81.40.Jj, 81.70.Bt

I. INTRODUCTION

Researchers in diverse fields[1–4]—such as materials science,[5] granular media,[6] structural and biomaterials engineering,[7] nondestructive evaluation,[8] and medical imaging[9]—have a strong interest in understanding the nonlinear mechanisms involved in the elastic response of solids to a dynamic excitation. However, the study of nonlinear phenomena (e.g., resonance frequency shift, harmonics generation, etc.) in materials as different as rocks,[10] granular media,[11] concrete,[12,13] composites,[14] ceramics,[15] bones, and other biological media,[9] is made extremely complex by the presence of nonequilibrium effects (i.e., conditioning, memory, and relaxation).

While features of the nonlinear elastic response of several materials are commonly recognized,[16] the distinction (and link) between nonlinearity and nonequilibrium[17] and the evidence of the rate dependence of hysteresis in quasistatic experiments[18] have revealed the issue to be even more complex. The most astonishing observation is that a dynamic excitation, low enough to avoid damage, causes a reduction in the elastic modulus (*softening*)[13,19,20] with a change in the elastic state of the material to a new, amplitude-dependent, equilibrium state (*conditioning*).[17,21] When the excitation is removed, *memory* of that elastic state is preserved, i.e., the elastic modulus does not return instantaneously to the initial value. In a long time, *relaxation* to the original elastic state occurs.[13]

The described interplay between nonlinearity (i.e., the dependence of a defined measurable quantity on the amplitude of the excitation) and nonequilibrium (i.e., the variation in the material parameters when the sample is excited at constant amplitude) is not captured by existing phenomenological models[22–27] which have been developed to describe elastic hysteresis in solids using a Preisach-Mayergoyz (PM) space approach.[28,29] Therefore, we propose (see Sec. II) a nondeterministic PM space model in which rate-dependent mechanisms are introduced to describe the phenomenology described in Refs. 13, 17, and 19.

The proposed model motivated us to design experiments in which effects due to nonlinearity and nonequilibrium can be separated. Therefore, a specific experimental analysis was implemented and predictions of the proposed model were verified on concrete samples (see Sec. III). The agreement between model predictions and experimental results is discussed as a validation of the approach proposed. Finally, the implications of our findings in the field of nonlinear elasticity are discussed in Sec. IV.

II. A MULTILEVEL MODEL

Elastic hysteresis in nonlinear media originates at the interface between linear homogeneous portions, separated by mesoscopic "interstitial" regions.[30,31] As shown in previous works, a suitable phenomenological modeling framework can be found in the PM space approach[28,29] in which the complex hysteretic behavior of such regions stems from the collective behavior of a large number of simple microscopic hysteretic elements (HEs). Within such framework, we introduce a stochastic PM space approach which allows the presence of nonequilibrium elastic states.

A. Model

In the model, the sample is discretized in a large number of cells ($i=1,\ldots,N$) arranged in series, each representing a mesoscopic element. Each cell is further divided into an ensemble of microscopic elements (HEs), which can reside in one of two different states. Constitutive equations of the mesoscopic cells are derived from simple equations of state defined for the HEs and discrete equations of motion describe the perturbations induced by a propagating elastic wave.

1. Constitutive equations for the microscopic elements

Each HE is described by the equation of state of a damped sticky spring, i.e., a spring (with elastic constant K) in parallel with a clapping element [see Fig. 1(a)]. It follows that the jth HE belonging to the ith cell can reside in one of the two following states [see Fig. 1(b)], depending on the stress level and on the load history:

(1) An elastic state (the HE behaves as a spring), where the stress (σ_{ij}) is proportional to the strain (η_{ij}),

$$\sigma_{ij} = K\eta_{ij} = K\frac{(l_{ij}-\delta)}{\delta}. \tag{1}$$

For simplicity, we assume that all HEs have the same rest length δ and elastic constant K. The generalization to springs

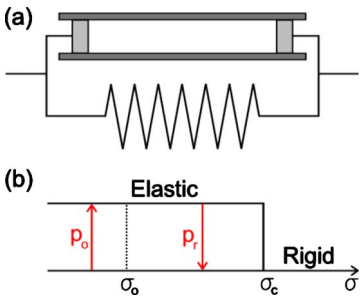

FIG. 1. (Color online) Schematic representation (a) of the sticky spring and (b) of its state vs pressure protocol. Arrows (red) denote potential transitions from one state to the other with related probabilities.

with different properties is straigthforward but more complex in notation. Here l_{ij} is the actual length of the spring.

(2) A rigid state (the HE behaves as a closed piston), where, independently from the stress, the strain becomes $\eta_{ij}=\sigma_c/K$. Here σ_c is the so-called closing pressure of the considered HE, defined below. The actual length of rigid HEs is

$$l_{ij} = \delta\left(1 + \frac{\sigma_c}{K}\right). \tag{2}$$

HEs continuously switch from one state to the other [see Fig. 1(b)]. When the HE is in the elastic state, the stress is supported by the spring of the element. When the stress becomes larger than the closing pressure σ_c, the two surfaces of the piston get in contact and the system becomes rigid. During the unloading process, when the stress supported by the piston falls below an opening pressure σ_o, the HEs may return to the elastic state with a given probability. The state of each of the HEs can be easily traced in time since the time evolution equations allow to define, at any time t, the spatial distribution of stresses within the sample.

The approach proposed here is that, rather than being deterministic as in existing models, the opening process occurs, for $\sigma \leq \sigma_o$, with a probability p_o. We assume p_o to be dependent on the difference between the closing and opening pressures $\Delta=\sigma_c-\sigma_o$. In fact, $\Delta \neq 0$ can be ascribed to some form of sticky mechanism between the surfaces forming the piston: the larger Δ is, the harder it is to break the "adhesion" and the lower is p_o. In principle, any function of Δ could be chosen to define p_o. Here, we use a Gompertz-type function,

$$p_o = \exp\{-\exp[(\Delta - p_{\max})/\tau]\}, \tag{3}$$

where τ is a constant and $p_{\max}$ is the maximum stress applied to the cell to which the HE belong.

On the contrary, transitions from the elastic to the rigid state occur when the two surfaces get in contact. Having such mechanism a different origin from sticky adhesion, the elastic to rigid transitions occur deterministically. The effects of introducing stochasticity in such transition can be studied as well but this is beyond the scope of the present contribution.

Finally, random transitions with probability p_r are also considered for pressures $\sigma_o<\sigma<\sigma_c$, where the two states are both possible [see Fig. 1(b)]. Such transitions account for stress fluctuations (e.g., due to thermal fluctuations), which can lead the stress to increase/decrease up to eventually reaching the closing/opening pressure. Since the transition to the elastic state is further governed by a probability p_o, it follows that the actual probability for a spontaneous rigid—elastic transition is $p_o p_r$, negligible if compared to the probability p_r. Of course, a dependence of p_r on the difference between the actual stress σ and σ_o (σ_c) could be expected but it is not implemented here. Indeed, in the present context, p_r does not have a significant role since it is mostly involved in the recovery effects, which are not analyzed here.

It is to be noted that for a relaxed specimen, the initial conditions, i.e., the states of the HEs at time 0, are determined by the described relaxation mechanisms. Indeed, the sample has been kept at stress equal to zero for a long time, therefore equilibrium has been reached. It follows that all HEs with $\sigma_o>0$ have had time to relax to the elastic state. Likewise, elements with $\sigma_c<0$ are in the rigid state. The remaining elements are subject to relaxation, hence they are distributed according to the relaxation probabilities. In particular, they are all in the rigid state, except for a portion given by the relative probability of a spontaneous transition from rigid to elastic: $p_r p_o/(p_r+p_r p_o)$. This number is small since p_o is small.

2. Behavior of a mesoscopic cell

Every mesoscopic cell i is built out of a series of microscopic HEs, some of which are elastic (springs) while the others are rigid. We recall that the length l_i of the cell is given by the sum of the lengths of its constituent elements,

$$l_i = \sum_j l_{ij} = \sum_{elastic} l_{ij} + \sum_{rigid} l_{ij}. \tag{4}$$

Assuming the stress to be in equilibrium within each mesoscopic cell, the stress σ_i over the ith cell is equal to the stresses σ_{ij} over each HE. Using Eq. (1), we have

$$\sum_{elastic} \sigma_{ij} = \sum_{elastic} \left(\frac{K}{\delta} l_{ij} - K\right) = \frac{K}{\delta} \sum_{elastic} l_{ij} - N_i^{el} K, \tag{5}$$

$$\sigma_i = \frac{1}{N_i^{el}} \sum_{elastic} \sigma_{ij}, \tag{6}$$

where N_i^{el} is the number of HEs in the elastic state at that pressure level. Combining Eqs. (5) and (6), we obtain

$$\begin{aligned}\sigma_i &= \frac{1}{N_i^{el}} \frac{K}{\delta} \sum_j l_{ij} - K - \frac{1}{N_i^{el}} \frac{K}{\delta} \sum_{rigid} l_{ij} \\ &= \frac{K}{N_i^{el}} \frac{\sum_j l_{ij} - N_i^{el}\delta - \sum_{rigid} l_{ij}}{\delta} \\ &= \frac{K}{N_i^{el}} \frac{l_i - M\delta - \sum_{rigid} (l_{ij} - \delta)}{\delta}.\end{aligned} \tag{7}$$

M is the number of HEs belonging to the cell. From Eq. (7), we can deduce that the equivalent elastic modulus E_i of the cell is stress dependent and, at a given pressure σ, it can be calculated as

$$1/E_i(\sigma) = N_i^{el}(\sigma)/K. \tag{8}$$

Finally, the stress of the cell can be obtained by knowing at each time the number of HEs in the elastic state and the total deformation of the rigid elements,

$$\lambda_i^c = \sum_{rigid} (l_{ij} - \delta). \tag{9}$$

We recall that the spring length is given by $l_i = \Sigma_j l_{ij} = u_{i+1} - u_i + \lambda$. Here u_i and u_{i+1} denote the displacements of the left and right tips of the cell while λ is the cell length, i.e., the distance between the tips at time 0. Note that $\lambda = M\delta$.

3. Macroscopic behavior of the sample

From the macroscopic point of view, the sample corresponds to a set of springs in series, each with a stress-strain constitutive equation given by Eq. (7). The equations of motion describing the tips of the springs are therefore the classical equations,

$$\rho \ddot{u}_i = \frac{\partial \sigma}{\partial x} = \frac{\sigma_i - \sigma_{i-1}}{\lambda}, \tag{10}$$

where ρ is the material density and a double dot denotes a second-order time derivative. Substituting Eq. (7) into Eq. (10), we obtain an equation which involves only the displacements,

$$\rho \ddot{u}_i = \frac{K}{\delta}\left[\frac{u_{i+1} - u_i + \lambda_i^c}{N_i^{el}} - \frac{u_i - u_{i-1} + \lambda_{i-1}^c}{N_{i-1}^{el}}\right]. \tag{11}$$

Equation (11) can be solved numerically using a finite-difference forward scheme for the temporal derivatives. Of course, at each time step, the number of HEs in the elastic state (N_i^{el}) and the total length of HEs in the rigid state (λ_i^c) must be calculated.

B. Model predictions

Let us consider a stress protocol $\sigma(t)$ and analyze the evolution of the number of elastic elements in a given mesoscopic cell. The behavior of the system is governed by $N_i^{el}(\sigma)$ [see Eq. (7)]; the HEs belonging to the cell are points in the PM space (σ_c, σ_o) since their closing and opening pressures can be considered as coordinates. They are distributed in a triangle $(\sigma_c > \sigma_o)$. The behavior of the mesoscopic cell is determined by the value of σ with respect to σ_o and σ_c [see Fig. 1(b)]. In the initial state, elements with $\sigma_o > 0$ and a very small portion of those with $\sigma_o < 0$ are in the elastic state [see upper-left plot of Fig. 2(a)]. Black (white) areas denote HEs in the rigid (elastic) state. When the stress increases (loading), transitions to the rigid state take place for HEs with $\sigma_c < \sigma$ [upper row of Fig. 2(a)]. When stress decreases [unloading, first two plots of the second row in Fig. 2(a)], σ must be compared with σ_o. All HEs above the horizontal line, i.e., with $\sigma_o > \sigma$, if rigid, become elastic with probability p_o. The regions depicted in gray and/or dotted, for a given value of σ, are therefore populated by a mix of elastic and rigid HEs.

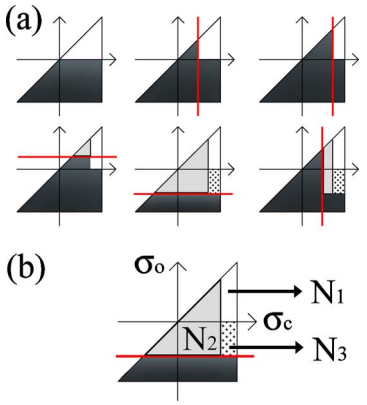

FIG. 2. (Color online) (a) PM space representation of the evolution of the distribution of HEs during loading (upper row) and unloading (first two plots of the lower row). White (black) colors represent areas occupied by HEs in the elastic (rigid) state. Grey and dotted areas are occupied by a mix of elastic and rigid HEs. (b) Elements in the white and black areas never change their state, those in the gray zone switch between the two states while those in the dotted area jump from rigid to elastic only.

As a consequence, when the stress varies in a given range, different areas of the PM space behave in different ways, as depicted in Fig. 2(b). Most of the HEs are not affected by the perturbation, namely, those in the white and black areas. Elements located in the gray triangle follow the perturbation, switching rapidly between the elastic and rigid states (p_o is large being σ_o close to σ_c), thus describing fast dynamic effects. Elements in the dotted rectangle do not follow the perturbation and can only be switched from the rigid to the elastic state. When the excitation amplitude is σ_1, the elastic modulus of the sample at pressure σ is approximately given by

$$1/E = (N_1 + N_2 + N_3)/K,$$

$$N_1 = \int_{\sigma_1}^{\infty} d\sigma_c \int_0^{\sigma_c} d\sigma_o \rho(\sigma_c, \sigma_o),$$

$$N_2 \sim \int_{\sigma}^{\sigma_1} d\sigma_c \int_{\sigma}^{\sigma_c} d\sigma_o \rho(\sigma_c, \sigma_o),$$

$$N_3 \sim \int_{\sigma_1}^{\infty} d\sigma_c \int_{-\sigma_1}^{0} d\sigma_o \rho(\sigma_c, \sigma_o) f(t), \tag{12}$$

where $f(t)$ is a function which increases with the duration t of the perturbation. The exact calculation of $f(t)$ is beyond the scope of this contribution. Only N_2 depends on the value of the actual stress while N_3 depends on the amplitude and duration of the excitation. Although both N_2 and N_3 contribute to the change in the elastic modulus, only N_2 has the

physical meaning of a nonlinearity. Indeed, N_3 relates to a transition to a new equilibrium state, which is softer than the initial one.

As a consequence of a stress protocol, the model predicts a semipermanent change (conditioning) in the elastic modulus of the sample in time (due to N_3). It corresponds to a slow process: the further the elements are from the gray triangle, the lower p_o is. This change becomes more and more evident by increasing the amplitude of the excitation and/or its duration. When the sample is excited for a long time at a large amplitude, the term N_3 saturates; all HEs in the corresponding rectangle become elastic and remain elastic also when returning to a lower excitation amplitude (memory), except for relaxing back over a long time with a time constant related to p_r (relaxation).

III. EXPERIMENTAL VERIFICATION

Laboratory experiments were performed to verify and discuss the properties of hysteretic media which emerge from the model discussed in the previous section. In particular, experiments have been designed to investigate the effects of the duration of the conditioning process, its consequences on nonlinear measurements and the existence of several conditioned states. We remark also that the results shown in Ref. 17 constitute as well a verification of our model. Indeed, the conditioning mechanism, i.e., the change in N_3 when the system is excited at a large amplitude, directly implies that the resonance frequency of the sample (at low amplitude) decreases after having perturbed the sample with a sinusoidal wave at a larger amplitude, as the experimental data of TenCate *et al.*[17] seem to indicate.

A. Experimental setup

We studied a linear (steel) and two nonlinear (concrete) cylinder-shaped samples, measuring 16 cm in height and 6 cm in diameter, each of them equipped with two identical piezoelectric transducers, with diameter of 4 cm. Transducers were coupled to the tips of the specimen with a thin layer of phenyl salicylate. The quality (and linearity) of the bonding and acquisition system, as well as the repeatability of measurements, were verified. The emitter was connected to a function generator through a linear amplifier; the function generator excited the transducer with a burst composed of 10 sine cycles at frequency $\omega_0=55.5$ kHz. Received signals were recorded with a sampling rate of 100 MSa/s with a time window of 1.3 ms. All experiments were conducted in a room at constant temperature and humidity.

We used the scaling subtraction method (SSM) (Refs. 32 and 33) to evaluate: (1) the global nonlinearity, defined as the dependence of a specific nonlinear indicator on the excitation amplitude. The SSM nonlinear indicator is defined as follows: a "linear" signal $v_{lin}(t)$ is defined as the output signal recorded using a low-amplitude excitation A_p; further signals $v_i(t)$ are recorded at higher excitation amplitudes A_i. For each measurement $v_i(t)$, a reference signal $v_i^{ref}(t)=(A_i/A_p)v_{lin}(t)$ and a SSM signal $w_A(t)=v_i(t)-v_i^{ref}(t)$ are defined.[32] If the material behaves linearly and its properties do not change in time, $w_A(t)$ is identically zero (except for noise effects) since for a linear material, the superposition principle can be applied. The SSM nonlinear indicator is then introduced as the "energy" of $w_A(t)$ over a time interval T,

$$\theta_A = 1/T \int_0^T w_A^2(t)dt. \tag{13}$$

(2) The conditioning effect, defined as the change in time of the response at a fixed excitation amplitude. In SSM measurements, the sample is excited with a repetition of bursts at constant amplitude. A signal $v_0(t)$ is measured as the response of the sample after the first burst excitation. Signals $v_i(t)$ are recorded after each burst (i is the burst index). Being the excitation always the same, the signal $w_i(t)=v_i(t)-v_0(t)$ should be identically zero (except for noise effects), if the material properties remain constant. Therefore, any change in the conditioning indicator θ_i [defined as the energy of the signal $w_i(t)$ as in Eq. (13)] represents a change in the Young modulus and/or attenuation.

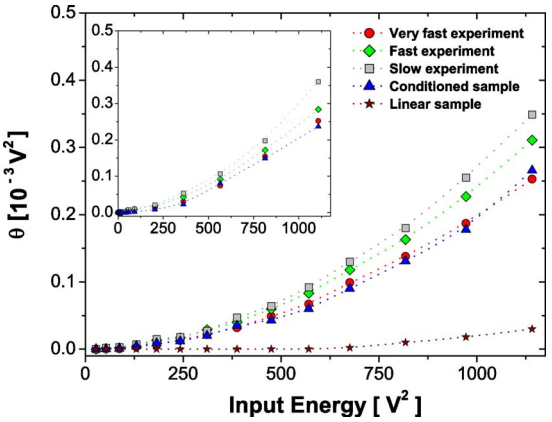

FIG. 3. (Color online) SSM indicator [Eq. (13)] vs excitation amplitude. Red circles: very fast experiment (one burst at each amplitude); green diamonds: fast experiment (20 bursts at each amplitude); black squares: slow experiment (100 bursts at each amplitude); blue triangles: slow experiment after a strong conditioning (sample conditioned at a large amplitude for 50 min before the experiment). Numerical simulations indicate a similar behavior as shown in the inset. No effect is noticed for a linear reference sample (steel): brown stars.

B. Global nonlinearity measurements

We studied the dependence of the measured nonlinearity on the duration of the experiment (see Appendix for more details about the implementation of the experiment). A very fast experiment was implemented as follows: the sample was excited with one single sinusoidal burst at each of 14 increasing amplitudes. Time lag between successive bursts was 10 s. The 14 output signals were recorded and processed, as discussed in Sec. III A. Since the duration of the experiment was very small, the system is expected not to have enough time to rearrange to a new equilibrium state. Results are reported in Fig. 3 (θ vs the energy of the injected signal; red circles). The increase in the SSM indicator reveals the presence of nonlinearity.

According to our model, nonequilibrium (conditioning) effects begin to play a relevant role when changing the duration of the experiment. On the same sample, after 1 week relaxation, a second (fast) experiment was conducted: 20 bursts (with a period of 10 s) were injected for each of the 14 amplitudes and output signals for each amplitude were recorded as the response of the system after the last burst of the series. The time lag between two successive amplitudes was 200 s. Results are reported as green diamonds in Fig. 3. Also, a "slow" experiment was performed by extending the number of bursts per amplitude to 100 (i.e., 1000 s time lag between successive amplitudes). Results are reported as black squares in Fig. 3. A longer excitation leads to a more pronounced nonlinearity because a long dynamic excitation leads to a transition to a new equilibrium state and this effect can be attributed to the increase in N_3 in Eq. (2). None of these effects can be observed in the linear sample (brown stars), thus confirming that they are not caused by the equipment.

Each experiment was repeated five times (after complete relaxation). Results were averaged, defining error bars with standard error theory and accounting for the precision of the instrumentation. Due to the excellent repeatability, error bars fall within symbol size.

Numerical simulations, based on the proposed model, were performed in the same conditions discussed above. Results (inset of Fig. 3) show an excellent agreement with the experimental observations, thus validating the proposed approach, even though a fit of the experimental data is not feasible since the one-dimensional model is only a first approximation of the two-dimensional real geometry.

C. Conditioning effects

The slow experiment was repeated, with an identical protocol as before (100 bursts per amplitude), immediately after having fully conditioned the sample. Full conditioning was obtained by exciting the specimen with a sequence of 300 bursts (total duration of about 50 min) at a constant amplitude. According to the model, nonequilibrium effects should here be negligible since conditioning was high/long enough to set the sample into the largest amplitude equilibrium already. Indeed, results shown in Fig. 3 (blue triangles) indicate that the same amount of nonlinearity is detected as in the very fast experiment conducted on the sample in its relaxed state. As in the very fast experiment, nonlinearity of the conditioned sample is due only to elements switching continuously from the rigid to the elastic state (N_2) since the contribution of "conditioned" elements (N_3) is the same for each excitation amplitude. The corresponding numerical simulations (blue symbols, inset of Fig. 3) agree with the experimental observations.

One last experiment was performed on another identical sample to show that the onset of a new equilibrium state is not instantaneous. The experimental protocol was designed as follows: (a) the sample was conditioned with a sequence of bursts at a constant high amplitude for 1 min with burst period of 4 s (i.e., 15 bursts) and output signals were recorded during the conditioning time; (b) the generator was switched off for about 80 s during which five repeated velocity measurements were performed using low-amplitude short rectangular pulse excitations. The two steps were repeated sequentially until the SSM indicator became almost constant, i.e., the specimen was in a new equilibrium state. The excitation protocol for conditioning is reported as a dotted line in Fig. 4. Results show a reduction in the elastic modulus (i.e., a decrease in the wave speed; blue triangles) and an increase in the θ indicator (black squares), which was calculated using the response recorded after the very first high-amplitude burst as reference signal. Since the excitation is the same but the response of the system varies (θ increases), the material properties (modulus and attenuation) are changing. This is a purely nonequilibrium effect since measurements are at constant amplitude. The indicator θ increases only while the excitation is on and after each resting period it restarts its rise from approximately the last value achieved. Velocities remain constant within each resting period and scattering of data gives an indication of the error bars. Simulation results are reported as red circles and are in excellent agreement with the experimental data. The temperature, measured on the surface of the sample using a thermocouple, is plotted vs time in Fig. 4 (green diamonds). It remains constant (except for small fluctuations) during the entire experiment, thus showing that our observations are not caused by heating of the sample.

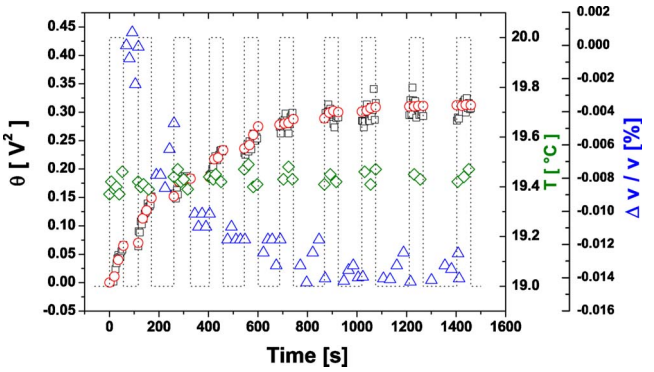

FIG. 4. (Color online) SSM indicator θ vs time during a conditioning experiment: the sample is excited with a series of bursts with constant high amplitude. The excitation protocol is alternately on and off in successive time intervals, as indicated by the dotted line. Numerical results (red circles) are in good agreement with experimental data (black squares). The trend of θ follows the evolution of the Young modulus in accordance with wave speed measurements (blue triangles). The temperature is constant apart from small fluctuations during the whole experiment (green diamonds).

IV. CONCLUSIONS

We have shown evidences of a strong interplay between nonlinearity and nonequilibrium in the elastic response of hysteretic media. Nonlinear measurements on fully conditioned samples seem not to be affected by nonequilibrium effects. Therefore conditioning the sample before performing nonlinear measurements could be a method to separate effects due to nonlinearity from those due to nonequilibrium. It

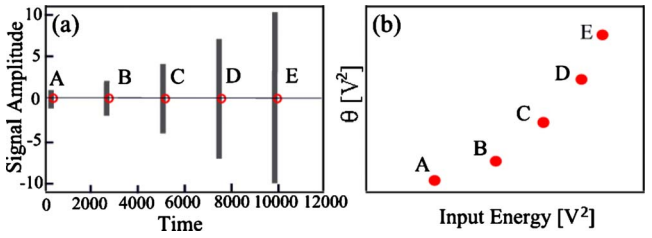

FIG. 5. (Color online) Schematic representation of the experimental acquisition in the case of a very fast experiment. (a) Sequence in time of the excitation. A given time lag passed before successive measurements, shown as red circles in the plot. (b) Each measurement provides a point in the plot θ vs input energy.

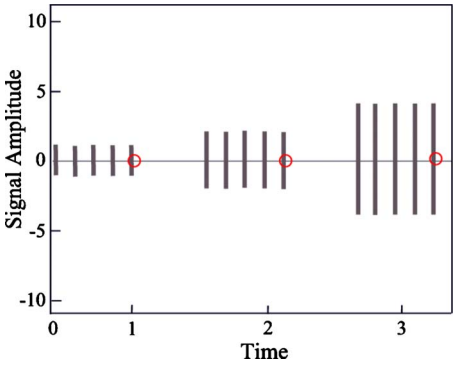

FIG. 6. (Color online) Schematic representation of the experimental acquisition varying the excitation duration (plot not in scale). Here, for each amplitude, the duration of the conditioning process corresponds to five bursts, each separated by a short time. Acquisition times are represented as red circles.

is important to note that the conditioning process induces reversible changes in the linear (and perhaps nonlinear) properties of the medium, which must still be globally understood. The effects shown cannot be captured without introducing in the model stochastic and/or time-dependent features.

Besides the importance of the proposed model to help understanding and interpreting the experimental data, we believe that several expectations in different fields are to be reconsidered in view of our results. Indeed, even though only concrete samples were tested here, similar observations are expected also for other nonlinear elastic materials (such as rocks) and perhaps for other hysteretic systems as well. As an example, softening induced by seismic/acoustic/ultrasonic excitations in materials, even close to collapse, can be a consequence of the material memory and not of damage progression as usually agreed. Thus softening induced by earthquakes[34] does not necessarily correspond to an increase in the soil nonlinearity. Also, the nonlinear response is dependent on the rate of the excitation protocol and on the preconditioning of the sample. Thus care has to be taken when comparing the nonlinearity of different samples in view of quantifying their relative amount of damage.[3,35,36]

APPENDIX

As mentioned in the text of the paper, one of the main goals of our study was to investigate the effects of the duration of conditioning on nonlinear ultrasonic measurements. In particular, as the proposed model predicts, several conditioned states are expected to take place, depending on the duration of the conditioning excitation. It follows that the duration of the conditioning process had to be carefully controlled during experiments, which could not be guaranteed by using continuous waves, such as in resonance experiments.

Therefore, in our study, the sample was excited by means of short bursts, each composed of a sequence of ten sinusoidal cycles centered at frequency 55.5 kHz. By using bursts, both the duration of the excitation (i.e., the number of injected bursts at each fixed amplitude) and the period between each successive burst (time between bursts) were easily controlled. The burst period was chosen large enough to avoid overlapping between successive bursts ($T=10$ s). In the paper, we refer to different experiments according to the extent in time of the conditioning wave, i.e., to the number of bursts injected per each amplitude. In particular, by simply varying the number of injected bursts, experiments have been classified as very fast, fast, and slow.

A schematic representation of a very fast experiment is shown in Fig. 5. For each defined amplitude (the total number of amplitudes was 5 in this example, each one marked with capital letters in Fig. 6), only one burst was injected: the duration of the conditioning excitation is thus very small. Between two successive bursts, the time lag was long enough to let the operator perform measurements and switch the function generator to the following amplitude.

The experiment was set as follows: (1) the generator is switched on at the lower excitation amplitude (A). Measurements are performed after burst A and the red dot in Fig. 1 denotes the measurement time. The temporal signal recorded is stored to be processed using the SSM and a point in the θ indicator vs input energy plot is drawn; (2) the excitation amplitude is increased (B) and the output signal is recorded, again, after the burst B. The corresponding point on the θ vs input plot is drawn. The procedure is repeated for each amplitude.

To increase the duration of conditioning and thus decrease the rate in order to perform the fast and slow experiments, the testing procedure was modified by sending a sequence of n bursts (as an example, $n=5$ in the schematic representation reported in Fig. 6), separated one another by a period T. Again, for each amplitude, output signals were measured after the last burst of the sequence, as schematically shown in Fig. 6 (red circle). After each measurement, the recorded signal was processed and a point in the θ indicator vs input energy plot was drawn.

By augmenting the number of periods composing the sequence of n bursts, any arbitrary duration of excitation can be programmed at the function generator. In the experiments discussed in Sec. III B, duration corresponding to 1 (very fast experiment), 20 (fast experiment), and 100 (slow experiment) bursts has been chosen.

[1] M. W. Barsoum, M. Radovic, T. Zhen, P. Finkel, and S. R. Kalidindi, Phys. Rev. Lett. **94**, 085501 (2005).
[2] J. Gomberg and P. A. Johnson, Nature (London) **437**, 830 (2005).
[3] K. Van den Abeele *et al.*, Res. Nondestruct. Eval. **12**, 17 (2000).
[4] A. Carpinteri, B. Chiaia, and P. Cornetti, Eng. Fract. Mech. **70**, 2321 (2003).
[5] T. J. Ulrich, A. M. Sutin, T. Claytor, P. Papin, P.-Y. Le Bas, and J. A. TenCate, Appl. Phys. Lett. **93**, 151914 (2008).
[6] C. Inserra, V. Tournat, and V. Gusev, Appl. Phys. Lett. **92**, 191916 (2008).
[7] J. C. Lacouture, P. A. Johnson, and F. Cohen-Tenoudji, J. Acoust. Soc. Am. **113**, 1325 (2003).
[8] I. Solodov and G. Busse, Appl. Phys. Lett. **91**, 251910 (2007).
[9] T. J. Ulrich, P. A. Johnson, M. Müller, D. Mitton, M. Talmant, and P. Laugier, Appl. Phys. Lett. **91**, 213901 (2007).
[10] R. A. Guyer, J. TenCate, and P. Johnson, Phys. Rev. Lett. **82**, 3280 (1999).
[11] P. A. Johnson and X. Jia, Nature (London) **437**, 871 (2005).
[12] C. Payan, V. Garnier, J. Moysan, and P. A. Johnson, J. Acoust. Soc. Am. **121**, EL125 (2007).
[13] M. Bentahar, H. El Aqra, R. El Guerjouma, M. Griffa, and M. Scalerandi, Phys. Rev. B **73**, 014116 (2006).
[14] R. El-Guerjouma, Adv. Eng. Mater. **3**, 601 (2001).
[15] K. Van den Abeele and K. Van den Velde, in *Review of Progress in Quantitative Nondestructive Evaluation: Volume 19*, AIP Conf. Proc. No. 509 (AIP, New York, 2000), p. 1359.
[16] R. A. Guyer and P. A. Johnson, Phys. Today **52**(4), 30 (1999).
[17] J. A. TenCate, D. Pasqualini, S. Habib, K. Heitmann, D. Higdon, and P. A. Johnson, Phys. Rev. Lett. **93**, 065501 (2004).
[18] K. E. Claytor, J. R. Koby, and J. A. TenCate, Geophys. Res. Lett. **36**, L06304 (2009).
[19] J. A. TenCate, E. Smith, L. W. Byers, and T. J. Shankland, in *Nonlinear Acoustics at the Turn of the Millennium: ISNA 15, 15th International Symposium*, AIP Conf. Proc. No. 524 (AIP, New York, 2000), p. 303.
[20] J. A. TenCate, E. Smith, and R. A. Guyer, Phys. Rev. Lett. **85**, 1020 (2000).
[21] D. Pasqualini, K. Heitmann, J. A. TenCate, S. Habib, D. Higdon, and P. A. Johnson, J. Geophys. Res. **112**, B01204 (2007).
[22] O. O. Vakhnenko, V. O. Vakhnenko, and T. J. Shankland, Phys. Rev. B **71**, 174103 (2005).
[23] C. Pecorari, J. Acoust. Soc. Am. **116**, 1938 (2004).
[24] P. P. Delsanto and M. Scalerandi, Phys. Rev. B **68**, 064107 (2003).
[25] M. Nobili and M. Scalerandi, Phys. Rev. B **69**, 104105 (2004).
[26] B. Capogrosso-Sansone and R. A. Guyer, Phys. Rev. B **66**, 224101 (2002).
[27] M. Scalerandi, P. P. Delsanto, and P. A. Johnson, J. Phys. D: Appl. Phys. **36**, 288 (2003).
[28] R. A. Guyer, K. R. McCall, and G. N. Boitnott, Phys. Rev. Lett. **74**, 3491 (1995).
[29] D. J. Holcomb, J. Geophys. Res. **86**, 6235 (1981).
[30] T. W. Darling *et al.*, in *Innovations in Nonlinear Acoustics: ISNA17 – 17th International Symposium on Nonlinear Acoustics including the International Sonic Boom Forum*, AIP Conf. Proc. No. 838 (AIP, New York, 2006), p. 19.
[31] V. Aleshin and K. Van den Abeele, J. Mech. Phys. Solids **53**, 795 (2005).
[32] M. Scalerandi, A. S. Gliozzi, C. L. E. Bruno, D. Masera, and P. Bocca, Appl. Phys. Lett. **92**, 101912 (2008).
[33] C. L. E. Bruno, A. S. Gliozzi, M. Scalerandi, and P. Antonaci, Phys. Rev. B **79**, 064108 (2009).
[34] J. L. Rubinstein, N. Uchida, and G. C. Beroza, J. Geophys. Res. **112**, B05315 (2007).
[35] C. Campos-Pozuelo, C. Vanhille, and J. A. Gallego-Juarez, IEEE Trans. Ultrason. Ferroelectr. Freq. Control **53**, 175 (2006).
[36] P. Antonaci, C. L. E. Bruno, P. G. Bocca, M. Scalerandi, and A. S. Gliozzi, Cem. Concr. Res. **40**, 340 (2010).